ARTICLE TYPE www.rsc.org/xxxxxx | XXXXXXXX

Proximal oxidation as a director of self organization

Giovanni Fois*[,a], Ciara T. Bolger[a,b], Justin D. Holmes[a,b] and Graham L. W. Cross[a,c]

Received (in XXX, XXX) Xth XXXXXXXXX 200X, Accepted Xth XXXXXXXXX 200X
First published on the web Xth XXXXXXXXX 200X
DOI: 10.1039/b000000x

Self organizing templates used as etch masks and growth seeds enable efficient mass fabrication of nanoscale device layers. In this work we introduce a new way to direct self-organisation of nanoscale pore formation during anodisation of metal layers of direct relevance to nanofabrication process flows. We demonstrate and quantitatively characterize how proximal surface oxidation frustrates and redirects random pore ordering in the film. Our results show a strict correlation between pore formation and oxide thickness on the aluminum surface providing important information on pore nucleation and growth in substrate-supported thin films and confirming the predictions of several existing theoretical models on pore growth. We find a linear relation between applied voltage and intrinsic self organizing interpore distance for supported thin films (from 80 to 150 nm) over a wide potential window between 40 and 120 V, mirroring behavior of thicker unsupported foils but with a different coefficient of proportionality. Using this technique, we are able to produce arbitrary and highly regular patterns of pores while manipulating pore pitch up to 20% from the natural spacing. This work demonstrates for the first time how local oxidation can direct self organisation.

Introduction

Integration of self organizing (SO) systems with semiconductor processing enables high resolution patterning of microelectronic circuit elements and offers a non-traditional pathway to performance improvements. Pore generation during anodisation of metals and block copolymer (BCP) micro-phase separation belong to a family of self organizing processes capable of generating regular, high precision nanoscale features over large areas. BCP-based lithography [1] features structure sizes down to the 7-10 nm [2-4] scale (although more typically at 20-40 nm [5]), and is generally compatible with familiar polymer resist processing techniques of electron beam lithography and photolithography. In terms of features, porous anodic oxides (PAO) do not exhibit the range of pattern morphologies possible in BCP systems; however they can match or exceed the dimensions for vertical pores in the sub-10 nm regime [6]. PAO films are substantially more mechanically and thermally stable than polymer films, making them compatible with harsher fabrication processes. Nevertheless, the integration of both SO systems with modern silicon technology requires external directing of the SO process via surface pre-patterning with electron beam lithography or molding techniques. BCPs generally form ordered domains with lateral dimensions of few microns while PAO with perfectly hexagonal patterns are obtained only on thick foils. A primary driver for this work is to demonstrate the potential of PAO as an alternative patterning technique suitable to thin film processing that can be implemented in mass manufacturing processes for nanotechnology. The only parallel technique reported, the nanoimprint related nanoindentation technique, has been shown only for thick films, and is likely to be difficult to implement in thin film geometries for several reasons. These include damage to substrate layers due to intense, long range indentation stress fields required to deform aluminium, and related parallelism requirements to achieve appropriate indentation stress on all indenters across large areas. This motivates the development of an industrially scalable "soft "process based on contact methods that do not involve high stress and should be amenable both conventional low pressure nanoimprint techniques with tip arrays or polymeric molds, as well as with scanned multiprobe tip lithography systems [7-8]. For the first time we show how local oxidation nanolithography (LON) can direct the self organisation of pores in PAO systems.

Atomic force microscope (AFM) nanolithography has generated considerable interest in the last decade because of the ability to create reproducible nanometric structures at room temperature and atmospheric pressure as well as the unique capabilities of imaging and positioning. LON is based on the spatial confinement of a chemical reaction within a nanometer-sized region defined by a combination of the probe-sample surface geometry and an external factor that could be an electric field or a liquid meniscus [9]. It has been demonstrated to be a versatile lithographic process capable of patterning a large number of material surfaces. Polymeric patterns with 2 nm resolution and 3 nm half pitch in ambient conditions [10] have been created on silicon substrates. Alternating nanostructures of octadecanethiol and decanethiol with full width at half maximum of 8 nm and lattice periodicity of 14 nm have been fabricated on Au surfaces by nanografting [11]. Dot arrays of oxide corresponding to bit density of terabit per square inch have been formed on silicon [12] and titanium [13] substrates. Straight oxide lines with widths of 13, 10 and 6 nm have been created respectively on Silicon [14], aluminium [15] and titanium [16]. The technological limitation due to the sequential character of the AFM technology can be upscaled via a parallel process using a solid support with multiple protrusions as a cathode. A stamp formed by a

mosaic of square regions characterized by parallel stripes of oxide 20 μm in length, 200 nm in width and 100 nm apart has been replicated on a silicon surface covering an area of 400 x 400 μm^2 in a process time of 1 minute [17]. Ultimate pitch resolution can be further pushed down as shown by a sibling technique, nanoimprint lithography (NIL). Austin and co-worker [18] showed the replica of 6 nm half pitch lines in a polymer resist using NIL. In this work, we apply the LON on aluminium thin films deposited on silicon substrates. We demonstrate for the first time how the oxide pattern grown through the LON process is capable of directing pore nucleation during anodisation.

We focus our study on anodic aluminum oxide (AAO), one of the most studied anodic oxide systems over the last forty years [19]. The pore self ordering process can be achieved with a two steps anodisation used under so called "mild anodisation" (MA) conditions [20] or "hard anodisation" (HA) process [21]. Both processes are characterized by a linear relation between the interpore distances and the applied voltage, and for oxalic acid gives an empirical relation of $D^{MA}=2.5(nm/V)*V$ for MA and $D^{HA}=2.0(nm/V)*V$ for HA. The disadvantage is that the self ordering is obtained only in narrow process windows, known as 'self ordering regimes'[22]. The synthesis of self ordered nanoporous alumina thin films on a silicon substrate by a two step process is not feasible due to the limited film thickness, which results in porous templates with a non-ordered arrangement [23] or formation of ordered domains with scale of few microns [24]. A more successful way to direct pore ordering in AAO films is to pre-pattern the aluminum surface prior to anodisation, where surface pre-texturing creates seeding points for pore development. Masuda *et al.* [25] first reported the creation of a highly ordered array of nanochannels in anodic alumina using a molding process to pre-pattern the surface of aluminum foils. Different techniques have also been used to pre-texture the surface, such as focused ion beam (FIB) for direct surface patterning [26] or electron beam lithography [27] validating this strategy. Also for thin aluminum films deposited on silicon, a promising method to achieve ordered array of pores is surface pre-texturing. Sander *et al.* [28] showed a well ordered hexagonal array of pores formed by anodising a 1.5 μm Al film evaporated onto a silicon substrate using a molding technique.

Our study is focused on the development of a pre-patterning technique capable of generating low stress on the substrates. At the same time, we demonstrate how the presence of oxide influences pore nucleation on the aluminium surface during the anodisation process. We use this finding to introduce a new soft patterning technique for thin supported aluminium films: a thin oxide grid is formed on the aluminium surface via a proximal electrical contact process capable of inducing pore ordering during anodisation. This method is consistent with mass manufacturing in thin film technology as no high residual stresses are involved and it will be implemented in the standard low pressure nanoimprint techniques. The process is shown to work over a wide range of applied voltage. For anodisation with oxalic acid from 40 to 120 V, a new linear empirical law is demonstrated for thin supported films that has a lower coefficient of proportionality than the well known constant for thick foils under similar anodisation conditions. These results show that the oxide plays an important role in the nucleation process during the first stage of pore development, providing new guidance for theoretical models.

Experimental

Substrate preparation

The substrates used in this work were 6 inch, p-type (100)-oriented silicon wafers (Si-Mat Silicon Materials) with resistivity in the range 1-6 Ω m. A 5 nm Titanium (Kurt J. Lescker, 99.995%) layer was evaporated on top at a rate of 0.02-0.04 nm/s with a Temescal FC-2000 Evaporation System to improve the adhesion of the subsequent electron beam evaporated 200 nm aluminium layer (Kurt J. Lescker 99.999%) with a deposition rate of 6 Å s^{-1}. The mean surface roughness (RMS) after the deposition was measured to be less than 2 nm on a 5 μm sq scanned area using an Asylum Research MFP-3D Atomic Force Microscope (AFM). (TEM cross section micrograph of the deposited film is shown in figure 1 of the electronic supplementary informations).

Pre-oxidation

The pre-oxidation process was performed with the Asylum Research MFP-3D AFM in contact mode under ambient air conditions with platinum/iridium coated electro levers model AC240s purchased by Asylum Research. The applied voltage on the tip was -10 V and all the patterns were realized with a scan velocity of 80 nm s^{-1}.

Anodisation

The patterned Al films were anodised in a custom-built anodisation cell. The substrates were immersed in 0.3 M oxalic acid (Fisher Scientific) at room temperature and anodised at a constant potential using a direct current (dc) power supply (Thurlby Thandar Instruments model EX752M). Platinum was employed as the counter electrode and the electrode separation distance was fixed at 6 cm. Samples with the same pre-oxidised structure were anodised at three different voltages: 40, 80 and 120 V.

Characterization

Porous samples were analyzed using a ZEISS Ultra scanning electron microscope (SEM) and an FEI Strata electron and ion dualbeam system. To improve the SEM image quality we reduced the surface charging by using a thin 4 nm layer of Palladium (Kurt J. Lescker, 99.95%) sputtered on the surface with a Cressington Sputter Coater 208 HR. The cross section image was taken with an FEI Titan transmission electron microscope (TEM) at 80kV. The TEM lamella was FIB cut following deposition of protective Pt layers on the porous surface; e beam deposition of a 200 nm Pt layer followed by ion assisted deposition of a further 2 um of Pt.

Results and discussion

Pre-oxidation patterning and anodisation

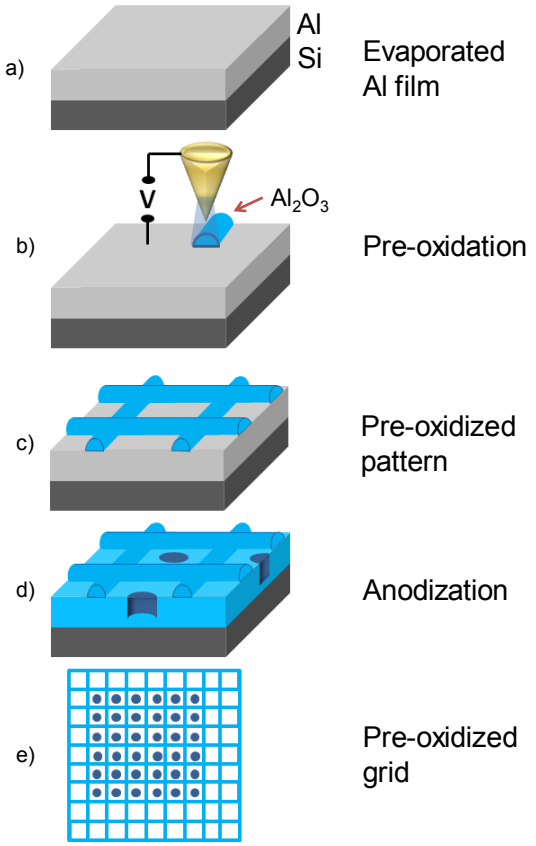

Fig. 1 Schematic of the pre-oxidation patterning process for aluminum thin film (gray) on silicon substrate (black): a square grid (e) pattern of aluminum oxide (blue) lines was created on the Al surface using contact mode electrical AFM with a conductive tip (b); the sample was then anodised with oxalic acid (0.3 M) at room temperature.

The anodization process of aluminum shows a linear relation between applied voltage and interpore distance, as discussed above. To direct self organisation, it is crucial that the pattern pitch matches the natural pore spacing for a given anodisation voltage.

Figure 1 shows a schematic of the process: after aluminium deposition (figure 1a), a high resolution pattern was created on the surface by passing a current through a scanning conductive AFM probe that induced local oxidation electrochemistry (figure 1b). Subsequently, the sample was anodised in oxalic acid 0.3M solution to achieve pore formation. Figure 1e shows an example of a grid pattern created on the Al film: a square grid of oxide lines (the blue lines in the image) was grown on the aluminum surface; the empty regions represent regions where only native oxide is present. The figure shows also a sample region that highlights where pores nucleate during the anodisation process: pores are forced to nucleate in between the pre-patterned oxide lines where the oxide is thinner. This will be further explained later in the paper.

The local oxidation was conducted in contact mode using a platinum/iridium coated tip which displays better resistance to wear with an applied load of 16 nN. Soft engagement is also necessary to minimise tip wear. From the literature it is well known that oxalic acid anodisation on aluminum produces porous templates with interpore distances between 100 and 200 nm [20,27] when applying voltages ranging from 40 to 80 V. The oxide patterns created on the surface have pitches ranging from 80 to 200 nm to match the natural pore spacing, as see above. The oxide lines need to be 70-80 nm width to have a well confined nucleation position. We choose to work in contact mode to easily achieve our goal without increasing the environment humidity and carrying out the experiment in ambient condition.

Figures 2 and 3 summarise the results of carrying out our process in practice. In figure 2a an AFM image of the oxide grid pattern created on the surface with a 100 nm pitch is displayed. The oxide lines formed by the patterning are about 80 nm in width and protrude about 3 nm from the surface (inset in figure 2a). We expect the inner oxide to be at a depth of approximately 10 nm [29] and the total oxide thickness to be no more than 15 nm. A TEM cross section (figure 3a) prepared by FIB milling shows the modulation of the aluminum oxide created on the aluminum surface. In the picture, the two regions with the thicker oxide represent the cross section profile of two consecutive oxide lines grown via the local oxidation process surrounded by regions with only the thin native oxide present. The shape of the oxide profile is not step-like but has a modulated profile with thick regions created by the LON process that gradually slope down. The patterned oxide lines are 13nm thick and 80 nm wide. The sample was anodised at 80 V for 5 minutes creating a porous film. After anodisation, evidence of the pre-oxidised lines was still present as shown in figure 2b, with the addition of highly visible pores at the surface. The perimeter of the square patterned region is marked with a red square in figure 2b. Figure 2c indicates the actual nucleation location of pores (outlined black circles) in the patterned region relative to the prescribed grid (blue lines) with 100 nm pitch. Pores nucleate in between oxide lines, in the regions where only the native oxide is present, following the order imposed by the pre-patterned grid and demonstrating a very high rate of order while disorder remains outside this region as shown outside the red square in figure 2b. The pores nucleated in between the pre-oxidised grid match the pattern with high fidelity. Figure 2d shows a magnified SEM micrograph of the bottom part of the pre-oxidised region shown in figure 2b. The pre-oxidised lines are clearly distinguishable respect to the random nucleation region. Focusing on nucleation positions, looking from the extending oxide lines toward the square region (in between red lines) it can be noted how pores nucleate only in regions between pre-oxidised lines, so where oxide is thinnest, while outside nucleation happens randomly. (Figure 2a in the electronic supplementary informations shows the same picture as in figure 2d with an example of oxide lines position (blue lines) highlighted respect to nucleation pore positions.) Further analysis of the ordering is provided by two-dimensional Fast Fourier Transform (2D FFT) of the pore locations (insets in figure 2b). The unpatterned region shows a broad but uniform circle reflecting the average disordered pore spacing, while a clear rectangular FFT pattern confirms the square symmetry of the pore lattice in the patterned region.

Critically, we find that the pores grow straight under the

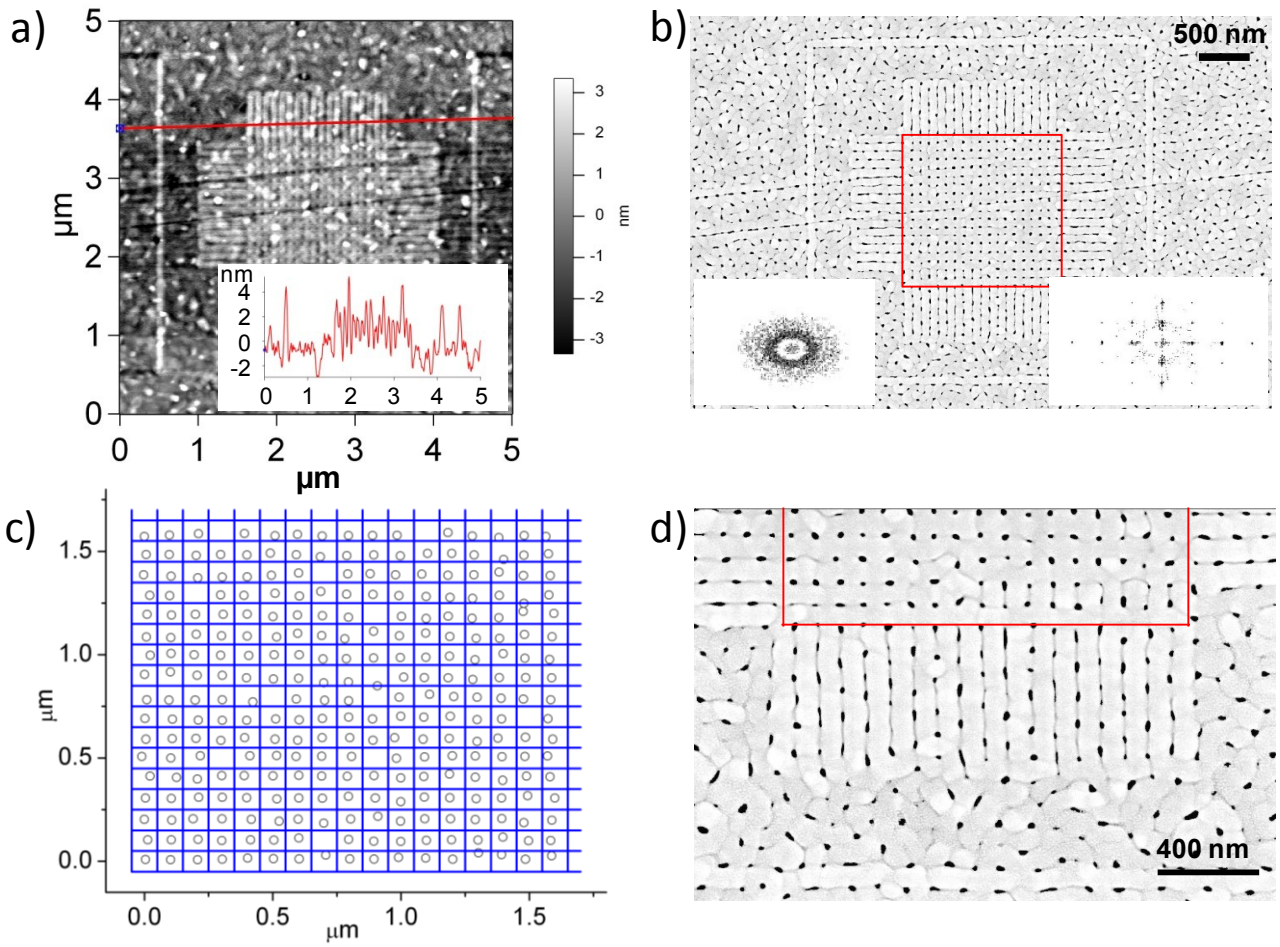

Fig. 2 Pore nucleation in pre-oxidised patterns after anodisation. a) AFM image of a pre-oxide grid with 100nm pitch formed on Al 200nm thick film and (inset) a line section showing the variation in oxide height of a few nanometers on the surface; b) SEM micrograph of the patterned area after anodisation with oxalic acid 0.3M at 80 V. The FFT image in the bottom right refers to the patterned area highlighted with the red square while the FFT in the top left refers to the unpatterned region; (c) the patterned area in picture (b) (red square) with the pore positions highlighted [31] using black empty circles, the blue lines in the figure represent the pre-patterned oxide grid with 100 nm pitch; d) SEM micrograph magnification of figure 2b).

nucleation points visible on the surface, as shown in the TEM image in figure 3b (in this image the visible layers are, from bottom to top, a titanium adhesion layer, the porous alumina, a palladium layer sputtered to improve the SEM imaging and finally an e-beam deposited platinum overlayer). The deposited aluminum film presents small grains as shown in the AFM image of the surface before anodisation (figure 2a). They are also very well visible after the anodisation process (figure 2b). The grains have an elongated shape and are approximately 200 nm long and 100 nm wide. The pores nucleate preferably in between two adjacent grains because concave surfaces aid local electric fields stronger than flat or convex surfaces [30]. The fact that the grain size is comparable with the interpore distance introduces a kind of structural disorder in the pore formation and an irregularity in the pore shape. The mouth of the pore as nucleated on the surface often appears distorted, i.e. elongated rather than perfectly circular, following the grain edge shape. The grain size comparable with the interpore distance introduces a kind of "noise" in the visual identification of pore positions and order. Image analysis then allows more accurate evaluation of pore ordering [31] as well as the introduction of an order parameter. The interpore distance was histogrammed [31]: figure 4 compares the histograms for the calculated distances between pores in the pre-patterned area (black line) and a non patterned area (red line) of the same sample. The black line shows a set of peaks at constant distances. The first peak, as indicated by arrows, relates to interpore distance between 100 and 150 nm, corresponding to the first neighbors distance in a square lattice with 100 nm pitch; the second peak is between 200 and 250 nm, corresponding to the second neighbors distance and so on. The unpatterned area, in contrast, shows only a slight peak at 100 to 150 nm reflecting short range (i.e. nearest neighbor) ordering, with no peaks visible at larger spacing.

The average interchannel distance was measured by analyzing the SEM images of unpatterned regions. In our thin film samples, we find that there is an increase in the mean interpore distance (D_{int}) and pore diameter (D_p) with increasing applied voltage, as reported in the thick foil literature. We measured a mean D_{int} of 80 nm, 120 nm and 150 nm, with an error of ±10 nm, for anodisation voltages of 40, 80 and 120 V respectively. The nanochannel diameter (D_p) was also measured directly on the surface. Mean D_p values for the three potentials were 25 ± 5 nm at 40 V, 40 ± 10 nm at 80 V and 70 ± 10 nm at 120 V.

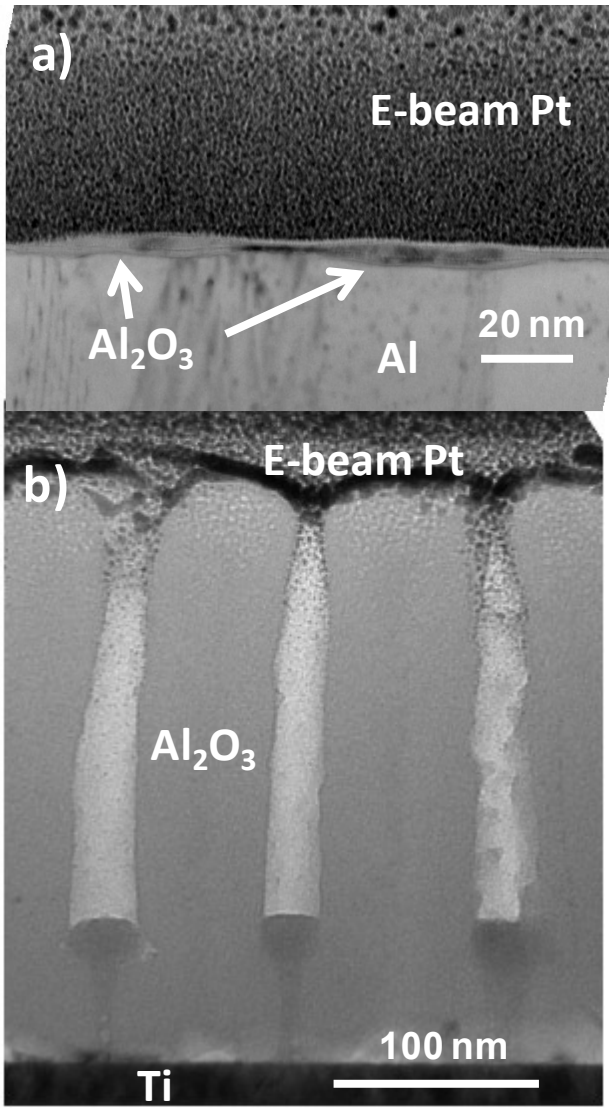

Fig. 3 a) **Patterned oxide profile:** TEM micrograph of a cross section taken on a pre-oxidised lines created on Al 200nm film: difference in thickness between pre-patterned oxide lines (arrows) and native oxide; b) **Straight pores:** a 200nm aluminum film anodised with oxalic acid at 80V.

Data analysis and discussion.

It is well known that the mechanism of nano-channel formation is an electrical field assisted dissolution of aluminium oxide formed during the anodisation process [30]. Over the last 40 years, researchers tried to explain both pore growth and self organisation as driven only by the external electric field. Jessensky *et al.* [34] in 1998 proposed that the formation of ordered hexagonal pore arrays is instead driven by the oxide flow along the pore walls generating mechanical stress at the metal/oxide interface due to the volume expansion of the aluminium during oxidation. Recently, Houser *et al.* [32] refined this argument explaining this oxide flow as generated by compressive stress at the pore base, which is due to the competition of strong anion adsorption with deposition of oxygen. These models are, unfortunately, not comprehensive and tend to focus on steady state growth as opposed to nucleation or growth termination. In this work, we assert that for a non-patterned, flat aluminum surface an

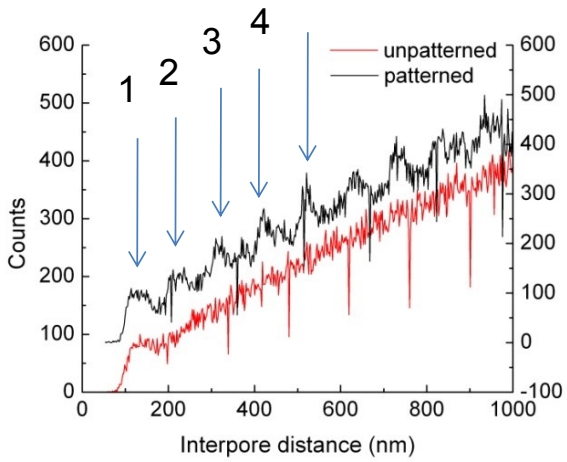

Fig. 4 Interpore distance. Histogram of the interpore distances for an unpatterned (red) and for the patterned (black) region in the same sample: peaks in the black data indicated by arrows are related to the induced order.

alumina pore nucleates during anodisation where the native oxide is thinner. The native aluminium oxide on an Al surface is known to be only a few nanometers thick, which makes proving this assertion difficult. Based on this idea, we have modified the surface oxide morphology of a thin Al film via proximal electrical contact. We have created surface regions where the oxide morphology is well known: as shown in figure 3a, oxide lines 13 nm thick surround square regions where only native oxide of 2-3 nm is present. After the anodisation process the pre-patterned oxide line profile is still visible on the surface giving a refence pattern for pore nucleation. In other words, as the oxide profile present on the surface is known before anodisation the pore nucleation positions can be studied with respect to oxide thickness inside the patterned regions. The precise mechanism for pore development in the first instant is still not understood. Before the steady state pore growth is reached, the system is in a non equilibrium state and the mechanisms occur quickly which makes probing of the processes very difficult. Nevertheless, our studies here with thin films provide important information about what happens during pore formation in the first few hundred nanometers of aluminum. Our results suggest that our original assertion, that pores nucleate where the oxide layer is thinner, is correct. An oxide layer of 10-15 nm is able to suppress pore nucleation during the anodisation process performed with oxalic acid in a window of applied voltage from 40 to 120 V. This is a key result for an exhaustive comprehension of the pore formation mechanisms. A complete theoretical model is still needed explaining nanochannels development from nucleation on the surface to steady state growth. A clear starting point for understanding pore nucleation arises from our results and the thickness of the native oxide present on the surface could play an important rule to achieve well ordered porous templates within thin films.

We have performed a comprehensive study of pore ordering as a function of oxide grid pitch and anodisation voltage: grid pitches ranged from 80 to 200 nm while applying three different potentials. We refer to each square enclosed by oxide lines in the pattern as a *grid position*. As shown before,

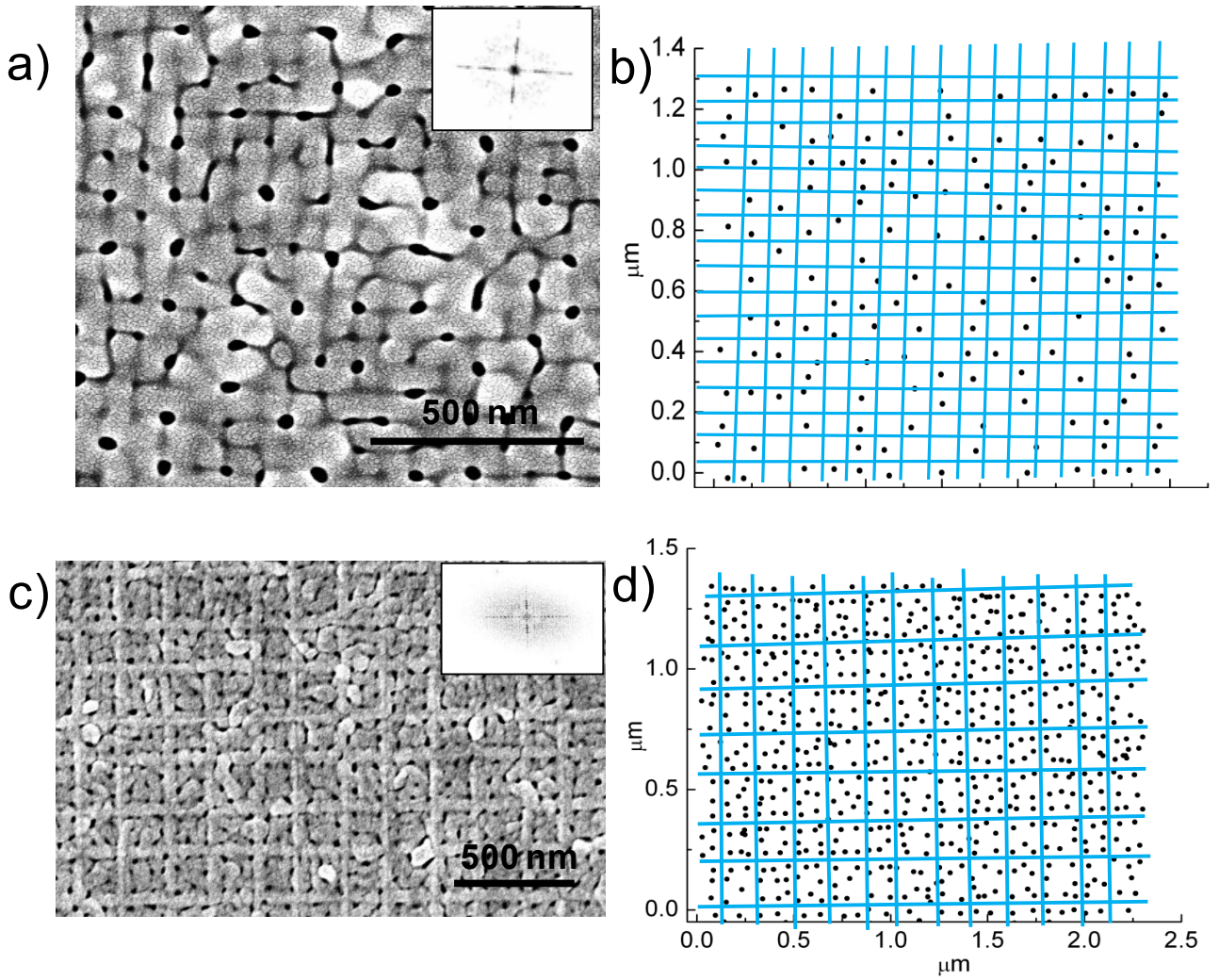

Fig. 5 Underfilling overfilling of pores in oxidation grids. a) (*Underfilling*) SEM micrograph of a 80nm pre-oxidised pitch after anodisation with oxalic acid at 120V. b) The same picture of (a) with pores centre positions highlighted [23] using black circles and the pre-patterned oxide grid represented by blue lines. c) (*Overfilling*) SEM picture of a 200nm pre-oxidised pitch after anodisation with oxalic acid at 40V. d) The same picture of (c) with pores centre positions highlighted [31] with black circles and the pre-patterned oxide grid represented by blue lines. The inset in (a) an (c) represent the FFTs of the same images.

these regions are characterized by the presence of only the thin native oxide on the surface, so a grid position also refers to a site of thin oxide. Using measurements of natural pore spacing in regions with no oxide grid present, we expect a perfect match between pattern and applied potential for values of 80 nm at 40 V, 120 nm at 80 V and 150 nm at 120 V. The 2D FFT analysis and the interpore distance histogram give two important ways to characterize pore order. From either of these we can derive an order parameter to evaluate the pattern matching. We call the fill parameter ξ the ratio between the actual number of pores formed in the patterned grid after anodisation, n_p and the number of available position in the grid, n_a : $\xi = n_p/n_a$. For anodisation potentials producing random pore spacing close to the pre-oxidation grid spacing, we expect perfect single pore filling at grid positions ($\xi = 1$). For higher potentials producing larger spacing we expect under filling ($\xi < 1$) of the available grid spots while for lower voltages we might expect over filling ($\xi > 1$). Either of the latter cases may lead to a loss of ordering.

In the case of under filling, the pores are prevented from nucleating in every position because the pattern pitch is shorter than the random interpore distance. This may occur because of a lack of room to accommodate the stress developed in the oxide volume expansion during the anodisation process between one pore and its neighbors [32,33]. In this case, pores can naturally jump from nucleating in the first neighbor position available to the second (or third and so on) neighbor position that allows a more suitable interpore distance for channel growth. Figure 5a shows a SEM image of a 80 nm pitch pre-oxidised pattern anodised with oxalic acid at 120 V. Pore positions in figure 5a are highlighted as black circles in figure 5b. The prescribed 80 nm pitch grid is shown as blue lines in the figure. Assessing the available positions in the array, pores do not nucleate in all sites but they skip from the first neighbor position to the second neighbor position because the distance between second neighbors is closer to the natural random spacing at the applied voltage. However, the overall arrangement of pores maintains a certain square order as shown by the FFT image in the inset of figure 5a.

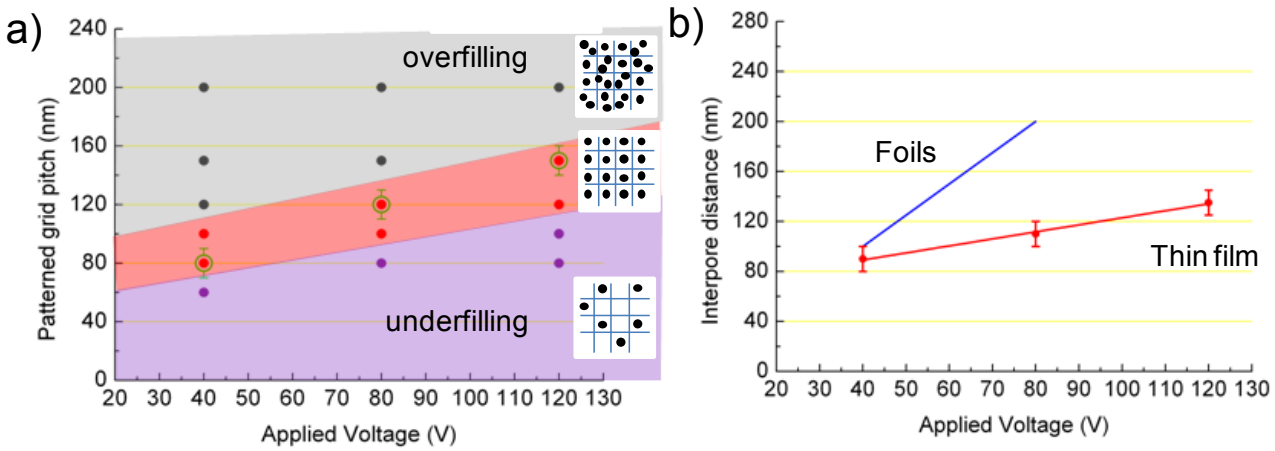

Fig. 6 a) Nature of pore ordering resulting from pre-oxidation grid pitch versus applied anodisation voltage: $\xi > 1$ overfilling (filled black circles), $\xi = 1$ perfect filling (filled red circles), and $\xi < 1$ underfilling (filled purple circles). As-measured thin film random interpore spacing vs. anodisation voltage is plotted with open green circles with error bars. A full description of the fill factor ξ is provided in the main text. b) Empirical law relating interpore distance and applied voltage for supported thin films (red line) and foils (blue line).

In the over filling case where $\xi > 1$, more than one pore nucleates in a single grid position as the patterned pitch greatly exceeds the natural pore spacing. Figure 5c shows the nucleation points for pores formed after anodisation with oxalic acid at 40 V on a surface with a pre-oxidised pattern with a grid pitch of 200 nm. The area in between the oxide lines for each position is sufficient to contain around 4 pores. Figure 5d highlights the position of the pores [31] as depicted with black circles, while the prescribed grid is shown by blue lines. Even in this case, a certain residual pore ordering remains present in the 2D FFT image in the inset of figure 5c. The crossed structure present in the FFT reflects an apparent pore preference to nucleate close to the pre-oxidised lines creating straight lines of nucleation. This can be seen also in figure 5a: for $\xi < 1$, a nucleation point jumps from one position to another in the grid but remains always confined in a pre-oxidised region. This behavior may be explained by the high electric field present in the oxide/metal interface forcing the dissolution process in the boundary zone. As suggested by O'Sullivan *et al.* [30], regions in the surface oxide that present irregularities with thinner oxide are characterized by an increasing gradient of electric field. The higher electric field induces more current and then higher dissolution in those regions enhancing the pore nucleation. Looking at the oxide profile on figure 3a, the oxide thickness decreases from the patterned line to the region where only native oxide is prensent and we expect an increasing gradient of the electric field in this transient region with the highest field value to be in the point where only native oxide is present. This explains why pores nucleate preferably close to patterned oxide lines.

Figure 6a summarises all the data acquired in this study. The patterned grid pitch is plotted against the applied voltage. Our measurements for the random interpore distance are reported with green empty circles; pitches showing a perfect match with applied voltage for which the fill parameter is $\xi = 1$ are represented with filled red circles; pitches with $\xi > 1$ are plotted with filled black circles and the other with $\xi < 1$ are shown as filled purple circles. Regions in which the underfilling and overfilling regimes occur are highlighted in light purple and light grey respectively. The region in which there is a perfect order is highlighted in light red. The order after anodisation in a pre-patterned grid with a pitch equal to the natural interpore distance is perfect, as expected. As shown in figure 6a, data for a 80 nm pitch at 40 V, a 120 nm pitch at 80 V and a 150 nm pitch at 120 V have $\xi = 1$. There is also a window of 20-30 nm around the "random" Dint value for which the order is still perfect. Examples are data for 100 nm pitch at 40 V, 100 nm at 80 V and 120 nm at 120 V for which the ξ value is still 1. Moving away from these values the order starts degrading. Increasing the pitch length, multipore nucleation per single position appears, the fill parameter becomes $\xi > 1$ and the system is in the "over filling" situation. The black circles indicate system conditions not allowing the perfect ordering: at 40 V for pitches longer than 120 nm, at 80 V for pitches longer than 150 nm and at 120 V for pitches longer than 200 nm. On the other hand, decreasing the pitch the system moves toward the under filling regime, jumps in the nucleation positions occur and the fill parameter becomes $\xi < 1$. This is the case for pitches of 60 nm or less at 40 V, 80 nm or less at 80 V and 100 nm or less at 120 V, represented with purple circles in the graph.

A linear relation between the applied voltage and the interpore distance was found for data with a fill parameter $\xi = 1$. A new empirical law for the anodisation with oxalic acid of supported thin aluminum films was found. Fitting data with a straight line we obtained the relation $D^{TF}=0.6(nm/V)*V$, where D^{TF} is the interpore spacing for thin films and V the applied voltage. The coefficient for the MA process of Al foils is about 5 times bigger. Figure 6b shows the comparison between the linear relation for thin supported aluminum films (red line) and for aluminum foils (blue line). The slope of the graph for the thin films is lower than that for the Al foils and, at a fixed applied voltage, the interpore spacing obtained after anodisation of a thin supported film is less than the pore distance obtained in anodised foils. The reason for this contraction in the interpore distance of the supported thin films is probably the effect of strain induced by the Si substrate in the film which is not present in the Al foils. The influence of the rigid Si substrate on the 200 nm Al film

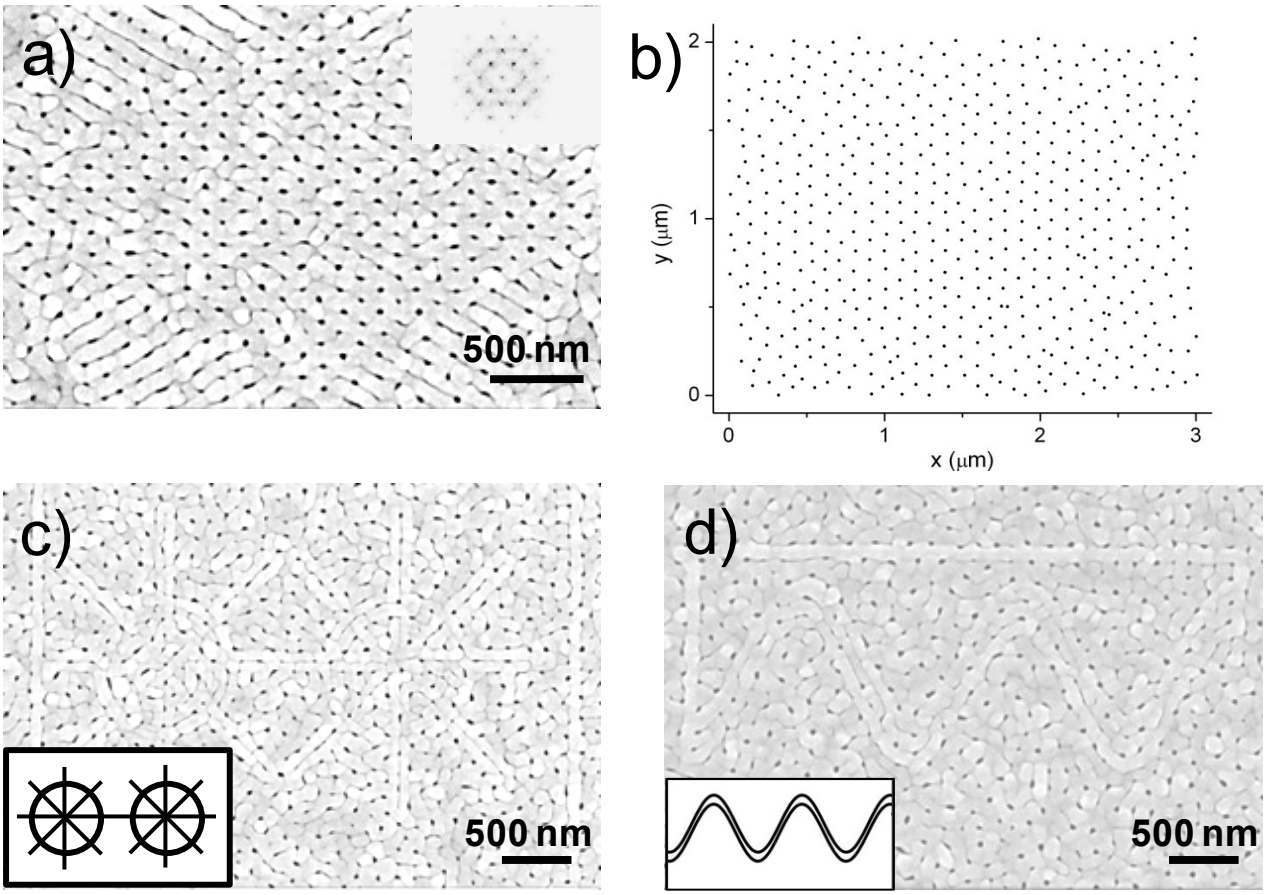

Fig. 7 SEM micrographs display aluminium films anodised with 0.3 M oxalic acid at 80 V. a) surface pre-patterned with a hexagonal oxide grid; b) the same picture of (a) with pores positions highlighted [23]: ordering is shown to be highly hexagonal as demonstrated by the FFT image in the inset of a); c) the inset shows the oxide pattern formed on this sample, the pores nucleate following the pre-oxidised lines; the same behavior is seen in d) where 2 sinusoids were realized.

deposited on top is a constriction in the volume expansion of the aluminum oxide formed in the anodisation process. The validity of this law is not restricted to narrow process windows as for the MA process of Al foils. We can define a working region extended in the voltage range between 40 and 120 V. At a fixed voltage, ordered templates are obtained inside a window of ± 15 nm around the related interpore distance. This means that, for a chosen applied voltage, an ordered pore array can be obtained not only for a pattern with pitch length equal to the random interpore distance but also for pitches greater or less than this, within a 30 nm window. The pores are constrained in a non-natural configuration because the interpore distance is higher/lower than the natural random distance. In other words, the system is forced to grow in a frustrated state in which the relative interpore distance is up to 20 % less than pores spacing in the non-patterned surface. During the anodisation process, thin films do not allow the self ordering rearrangement of the pores because the process occurs over a very short time period so pores grow vertically, immediately under the nucleation point (figure 3b), following the order imposed by the pre-patterned grid. This new feature introduces more flexibility in nanotechnology manufacturing allowing the creation of structures with different pitches without changing the applied voltage in the anodisation process. Our results show that pre-oxidation patterning of aluminum films is a successful method to drive pore nucleation in the anodisation process. Pores are confined within regions delimited by the oxide lines formed during the pre-patterning process and do not nucleate along the pre-oxidised lines. In this work, we have created ordered square arranged pores arrays. The pre-oxidation patterning induces pore formation in a non-natural arrangement but following the empirical rule for thin film anodisation, defined previously. We confirmed that our method also works to create hexagonally ordered pore arrays, as shown by the SEM image in figure 7a, the hexagonal array in the FFT image shown in the inset confirms the perfect arrangement. In the same way, unusual patterns can be realized by forcing the pores to nucleate along preferred directions. An example is shown in figure 7c: the surface was pre-oxidised by drawing the pattern showed in the inset: Two circles of 1 μm diameter crossed in the centre by two crosses tilted by 45° to each other and 2 μm long. Each line was formed by creating two parallel oxide lines at a separation distance of 90 nm. The sample was anodised with oxalic acid at 80 V and the SEM micrograph shows clearly the pores nucleated in between the pre-oxidised lines, following both the straight lines and the circles. Another example is shown in figure 7c: two sinusoids were patterned on the surface. The SEM image was taken after anodisation at 80 V and shows pores nucleate following the pre-patterned oxide lines.

Conclusions

In summary, we show how proximal oxidation can direct self

organisation during the anodisation process. The aluminum surface was chemically modified via a local oxidation process achieved with a conductive AFM tip. Square grids containing ~15 nm thick oxide lines at different pitches were created on the Al surface. The pre-oxidised patterns have the capability to control and frustrate pore nucleation and induce pore ordering during the anodisation process with oxalic acid for applied voltage in the range of 40 – 120 V. We have studied pore nucleation in thin aluminum films deposited on silicon substrates and for the first time we have demonstrated a direct relation between aluminum oxide thickness present on the surface and pore nucleation. This result is an important starting point for understanding of the nucleation mechanisms of pores in the anodisation process and suggests that, for a flat surface, a pore nucleates where the native oxide is thin. Further studies are required to better understand the influence of reducing the oxide thickness in the pre-patterning process. Changing the experimental parameters such as applied potential, scan speed and environmental humidity is likely to allow increased control over the patterning process and to study the limits of this technique. We confirm that the empirical law relating applied voltage to interpore distance during anodisation process in thin supported films is linear as for the well known relation in the MA and HA processes using Al foils. The new linear coefficient for thin films has found to be lower than for MA and HA processes. This means that the interpore spacing in porous alumina produced by anodisation of thin films is lower than the interpore distance obtained by anodisation Al foils with either MA or HA process, for fixed the experimental parameters. The silicon substrate induces mechanical strain in the thin film constraining the interpore distance. We have developed a new pre-patterning technique to control pore nucleation during the anodisation of thin aluminum films evaporated on silicon substrates demonstrating that a high level of ordering can be achieved with this new soft process. This technique allows a low stress, scalable and flexible process suitable to mass manufacturing which could be implemented with tip array technology, scanned multiprobe tip lithography systems, as well as standard soft imprinting techniques.

Acknowledgments

The authors thank Mr. Tarek Lutz and Mr. Cathal McAuley for the help in the TEM samples preparation, Dr. Markus Boese for the TEM images and the Advanced Microscopy Laboratory for the technical assistance. We acknowledge financial support from CRANN/SFI (Project 08-CE-I1432) and the Irish Research Council for Science Engineering and Technology (IRCSET) for the studentship to CB. This research was also enabled by the Higher Education Authority Program for Research in Third Level Institutions (2007-2011) via the INSPIRE program.

Notes and references

[a] *Centre for Research on Adaptive Nanostructures and Nanodevices (CRANN), Trinity College Dublin, Dublin 2, Ireland*
Fax: +353 1 896 3037; Tel: +353 1 896 4628; E-mail: foisg@tcd.ie
[b] *Materials and Supercritical Fluids Group, Department of Chemistry and the Tyndall National Institute, University College Cork, Cork, Ireland*
[c] *School of Physics, Trinity College Dublin, Dublin 2, Ireland.*

1 H. Sai, H. Fujii, K. Arafune, Y. Ohshita and M. Yamaguchi *Appl. Phys. Lett.*, *2006*, **88**, 201116.
2 S. M. Park, O. H. Park, J. Y. Cheng, C. T. Rettner and H. C. Kim *Nanotechnology 2008*, **19**, 455304.
3 J. K. Bosworth, M. Y. Paik, R. Ruiz, E. L. Schwartz, J. Q. Huang, A. W. Ko, D. M. Smilgies, C. T. Black and C. K. Ober *Acs Nano 2008*, **2**, (7), 1396-1402.
4 S. Park, D. H. Lee, J. Xu, B. Kim, S. W. Hong, U. Jeong,T. Xu and T. P. Russell *Science 2009*, **323**, 1030-1033.
5 M. S. Park, M. P. Stoykovich, R. Ruiz, Y. Zhang, C. T. Black and P. F. Nealey *Adv. Mater. 2007*, **19**, 607-611.
6 S. Z. Chu, K. Wada, S. Inoue and S. Todoroki *Chem. Mater.* **2002**, *14*, 4595-4602.
7 NanoInk Company products (parallel tip arrays), http://www.nanoink.net/
8 P. Vettiger,G. L. W. Cross,M. Despont,U. Drechsler,U. Dürig, B. Gotsmann, W. Häberele, M. A. Lantz, H. Rothuizen,R. Stutz, *et al*. The "Millipede"—Nanotechnology Entering Data Storage. *IEEE Trans. Nanotechnol. 2002*, **1**, 39–55.
9 R. Garcia, R. V. Martinez and J. Martinez *Chem. Soc. Rev. 2005*, **35**, 29-38.
10 R. V. Martinez,N. S. Losilla, J. Martinez, Y. Huttel and R. Garcia *Nanoletters 2007*, **7**, 1846-1850.
11 J. F. Liu, J. R. Von Ehr, C. Baur, R. Stallcup, J. Randal and K. Bray *Appl. Phys. Lett. 2004*, **84**, 1359-1361.
12 R. Garcia, M. Calleja and H. Rohrer *J. Appl. Phys. 1999*, **86**, 1898-1903.
13 Cooper E B, Manalis S R, Fang H, Dai H, Matsumoto K, Minne S C, Hunt T and Quate C F *Appl. Phys. Lett.*, **1999**, *75*, 3566-3568.
14 M. Calleja and R. Garcia *Appl. Phys. Lett. 2000*, **76**, 3427-3429.
15 Z. J. Davis, G. Abadal, O. Hansen, X. Borisè, N. Barniol, F. Pèrez-Murano and A. Boisen *Ultramicroscopy*, *2003*, **97**, 467-472.
16 Y. Gotoh, K. Matsumoto, T. Maeda, E. B. Cooper, S. R. Manalis, H. Fang, S. C. Minne, T. Hunt, H. Dai, J. Harris *et al. J. Vac. Sci. Technol. A 2000*, **18**, 1321-1325.
17 J. Martinez, N. S. Losilla, F. Biscarini, G. Schmidt, T. Borzenko, W. Molenkamp and R. Garcia *Rev. Sci. Instrum. 2006*, **77**, 086106.
18 M. D. Austin, W. Zhang, H. Ge, D. Wasserman, S. A. Lyon and S. Y. Chou *Nanotechnology 2005*, **16**, 1058-1061.
19 J. W. Diggle, T. C. Downie and C. W. Goulding *Chem. Rev. 1969*, **69**, 365-405.
20 H. Masuda and K. Fukuda *Science 1995*, **268**, 1466-1468.
21 W. Lee, R. Ji, U. Gösele and K. Nielsch *Nature Mater. 2006*, **5**, 741-747.
22 A. L. Friedman, D. Brittain and L. Menon *J. Chem. Phys. 2007*, **127**, 154717.
23 M. S.Sander and L. S. Tan *Adv. Funct. Mater. 2003*, **13**, 393-397.
24 A. Cai, H. Zhang, H. Hua and Z. Zhang *Nanotechnology 2002*, **13**, 627-630.
25 H. Masuda, H. Yamada, H. Satoh, H. Asoh, M. Nakao, T. Tamamura *Appl.Phys. Lett. 1997*, **71**, 2770-2772.
26 C. Y. Liu, A. Datta and Y. L. Wang *Appl.Phys. Lett. 2001*, **78**, 120-122.
27 A. P. Li, F. Müller and U. Gösele *Electrochem. Solid- State Lett. 2000*, **3**, 131-134.
28 M. S. Sander, J. M. Côté, W. Gu, B. M. Kile and C. P. Tripp *Adv. Mater. 2004*, **16**, 2052-2057.
29 A. Notargiacomo, E. Giovine, F. Evangelisti, V. Foglietti and R. Leoni *Materials Science and Engineering C 2002*, **19**, 185-188.
30 J. P. O'Sullivan and G. C. Wood *Proc. Roy. Soc. 1970*, ***A317***, 511-543.

31 SEM images were analyzed using a custom-made software written with LabView 7.1 to find the centroid coordinates for each pore, points are replotted using black circles in a white matrix to highlight pore position. The same LabView software was used to calculate the distance between one pore and the other. Distance was calculated only once and histograms were obtained at the end of the process.
32 J. E. Houser and K. R. Hebert *Nature Mater. 2009*, **8**, 415-420.
33 V. P. Parkhutik and V. I. Shershulsky *J. Phys. D: Appl. Phys. 1992*, **25**, 1258-1263.
34 O. Jessensky, F. Müller and U. Gösele *Appl.Phys. Lett. 1998*, **72**, 1173-1175.